

Magnetic and electronic properties of two-dimensional metal-organic frameworks $TM_3(C_2NH)_{12}$

Zhen Feng(冯振), Yi Li(李依), Yaqiang Ma(马亚强), Yipeng An(安义鹏), and Xianqi Dai(戴宪起)
Citation: Chin. Phys. B, 2021, 30 (**9**): 097102. DOI: 10.1088/1674-1056/ac0cdb
Journal homepage: http://cpb.iphy.ac.cn; http://iopscience.iop.org/cpb

What follows is a list of articles you may be interested in

Electronic structures of vacancies in $Co_3Sn_2S_2$

Yuxiang Gao(高于翔), Xin Jin(金鑫), Yixuan Gao(高艺璇), Yu-Yang Zhang(张余洋), and Shixuan Du(杜世萱)
Chin. Phys. B, 2021, 30 (**7**): 077102. DOI: 10.1088/1674-1056/abfa05

Tuning transport coefficients of monolayer $MoSi_2N_4$ with biaxial strain

Xiao-Shu Guo(郭小姝) and San-Dong Guo(郭三栋)
Chin. Phys. B, 2021, 30 (**6**): 067102. DOI: 10.1088/1674-1056/abdb22

Investigation of electronic, elastic, and optical properties of topological electride Ca_3Pb via first-principles calculations

Chang Sun(孙畅), Xin-Yu Cao(曹新宇), Xi-Hui Wang(王西惠), Xiao-Le Qiu(邱潇乐), Zheng-Hui Fang(方铮辉), Yu-Jie Yuan(袁宇杰), Kai Liu(刘凯), and Xiao Zhang(张晓)
Chin. Phys. B, 2021, 30 (**5**): 057104. DOI: 10.1088/1674-1056/abec38

Interfacial properties of g-C_3N_4/TiO_2 heterostructures studied by DFT calculations

Chen-Shan Peng(彭春山), Yong-Dong Zhou(周永东), Sui-Shuan Zhang(张虽栓), and Zong-Yan Zhao(赵宗彦)
Chin. Phys. B, 2021, 30 (**1**): 017101. DOI: 10.1088/1674-1056/abb30b

First-principles study of magnetism of 3d transition metals and nitrogen co-doped monolayer MoS_2

Long Lin(林龙), Yi-Peng Guo(郭义鹏), Chao-Zheng He(何朝政), Hua-Long Tao(陶华龙), Jing-Tao Huang(黄敬涛), Wei-Yang Yu(余伟阳), Rui-Xin Chen(陈瑞欣), Meng-Si Lou(娄梦思), Long-Bin Yan(闫龙斌)
Chin. Phys. B, 2020, 29 (**9**): 097102. DOI: 10.1088/1674-1056/ab9741

SPECIAL TOPIC — Two-dimensional magnetic materials and devices

Magnetic and electronic properties of two-dimensional metal-organic frameworks $TM_3(C_2NH)_{12}$*

Zhen Feng(冯振)[1,2], Yi Li(李依)[1], Yaqiang Ma(马亚强)[1], Yipeng An(安义鹏)[1,†], and Xianqi Dai(戴宪起)[1,‡]

[1] School of Physics, Henan Normal University, Xinxiang 453007, China
[2] School of Materials Science and Engineering, Henan Institute of Technology, Xinxiang 453000, China

(Received 20 April 2021; revised manuscript received 7 June 2021; accepted manuscript online 21 June 2021)

The ferromagnetism of two-dimensional (2D) materials has aroused great interest in recent years, which may play an important role in the next-generation magnetic devices. Herein, a series of 2D transition metal-organic framework materials (TM-NH MOF, TM = Sc–Zn) are designed, and their electronic and magnetic characters are systematically studied by means of first-principles calculations. Their structural stabilities are examined through binding energies and *ab-initio* molecular dynamics simulations. Their optimized lattice constants are correlated to the central TM atoms. These 2D TM-NH MOF nanosheets exhibit various electronic and magnetic performances owing to the effective charge transfer and interaction between TM atoms and graphene linkers. Interestingly, Ni- and Zn-NH MOFs are nonmagnetic semiconductors (SM) with band gaps of 0.41 eV and 0.61 eV, respectively. Co- and Cu-NH MOFs are bipolar magnetic semiconductors (BMS), while Fe-NH MOF monolayer is a half-semiconductor (HSM). Furthermore, the elastic strain could tune their magnetic behaviors and transformation, which ascribes to the charge redistribution of TM-3d states. This work predicts several new 2D magnetic MOF materials, which are promising for applications in spintronics and nanoelectronics.

Keywords: two-dimensional metal-organic frameworks, electronic structure, magnetic property, strain engineering

PACS: 71.15.Mb, 73.22.–f, 73.40.Vz **DOI:** 10.1088/1674-1056/ac0cdb

1. Introduction

Compared with bulk materials, two-dimensional (2D) materials exhibit many unique characters in mechanical, electrical, optical, and thermal properties. Therefore, many scientists make enormous effects to explore the new family of 2D nanomaterials,[1,2] which could display metallic, semiconducting, superconducting, insulating, thermoelectric, and ferroelectric properties.[3–6] However, most 2D materials exhibit a nonmagnetic ground state, suggesting that they are different to be utilized as spintronic devices and magnetic recording materials due to the prerequisite requirements of magnetism.

Usually, the electronic and magnetic characters of pristine 2D monolayers could be tuned and introduced by absorbing and doping transition metal (TM) atoms. This approach has been successfully realized in series of 2D monolayers, including graphene,[7,8] graphyne,[9] arsenene,[10] h-BN,[11,12] and phosphorene.[13] Another side, some intrinsic magnetic 2D materials such as CrI_3,[14] $Cr_2Ge_2Te_6$,[15] $MnBi_2Te_4$,[16] and Fe_3GeTe_2[17–19] have been experimentally discovered and investigated, which have potential applications in high-density data storage and nano-spintronic devices.[20,21] For instance, the spin polarization of half-metallic (HM) ferromagnets could reach 100%, due to the single spin state characteristics, i.e., one spin state is metallic conduction while the other state is semiconducting. The HM magnets are important in some cases, such as spin-filters and spin-polarized scanning tunneling microscope. Half semiconductors (HSC) are characterized by unique spin states that valence band maximum (VBM) and conduction band minimum (CBM) come from the same spin state. For bipolar magnetic semiconductors (BMS), VBM and CBM consist of opposite spin states, indicating that they could apply in spin injection and generation.[22,23] These promising applications drive more scientists to explore the 2D magnetic nanomaterials.

The 2D metal-organic frameworks (MOF) are porous hybrid materials consisting of transition metal nodes and organic ligands, and a recent class of magnetic materials.[24–26] Transition metal atoms are periodically connected with the organic ligands in MOF materials, inducing charge redistribution and strong interaction between them. These are beneficial to the stability of the framework structures. Recently, a series of 2D MOF nanomaterials were experimentally synthesized. For instance, $M_3C_{12}X_{12}$ and $M_3C_{36}H_{12}X_{12}$ systems (M = transition metal atoms, X = O, S, and NH).[21,27–31] Scientists are pay-

*Project supported by the National Natural Science Foundation of China (Grant Nos. 62074053, 61901161, 21906041, and 11774079), the Natural Science Foundation of Henan Province, China (Grant Nos. 202300410226, 202300410237, and 202300410100), Henan Overseas Expertise Introduction Center for Discipline Innovation (Grant No. CXJD2019005), and key scientific research projects of Colleges and universities in Henan Province, China (Grant Nos. 21A480004, 152102210306, 192102310499, and 19B450001).

†Corresponding author. E-mail: ypan@htu.edu.cn
‡Corresponding author. E-mail: xqdai@htu.edu.cn

© 2021 Chinese Physical Society and IOP Publishing Ltd

ing more and more attention to these interesting lattice structures, they are seeking more MOF candidates using similar chemical reactions and theoretical investigations. For example, Rabczuk *et al.* found that Ag, Cu, Cr, and $MnC_{12}(NH)_{12}$ 2D MOF monolayers exhibit half-metallic characters, suggesting that they are promising candidates for spintronics.[32] Sarkar *et al.* proposed several 3d transition metals based on the $M_3C_{12}S_{12}$. They found that $Cr_3C_{12}S_{12}$ exhibits spin-liquid, whereas $Co_3C_{12}S_{12}$, $Fe_3C_{12}S_{12}$, and $Mn_3C_{12}S_{12}$ are ferromagnetic half-metals.[33,34] Zhao *et al.* found that $Mn_3C_{12}S_{12}$ monolayer exhibits a half-metallic performance, and its Curie temperature is about 200 K by using the Ising model. The $Mn_3C_{12}S_{12}$ monolayer possesses a nonmagnetic ground state and a SOC band-gap reaching 2.4 meV, indicating that it may achieve the quantum anomalous Hall effect.[35] A similar atomic structure, $Mn_3C_{12}N_{12}H_{12}$ monolayer was predicted by Sun *et al.* The calculated results showed that the p–d exchange interactions could more effectively mediate the magnetic couplings, which results in a high Curie temperature of 450 K.[36] Very recently, Feng *et al.* reported a magnetic 2D Fe-PTC MOF material, which was synthesized from the reaction of 1,2,3,4,5,6,7,8,9,10, 11,12-perthiolated coronene (Fe-PTC) with ammoniacal solutions of iron acetate.[37] The variable temperature conductivity measurements revealed that the 2D Fe-PTC MOF pellets display a typical semiconducting character and a room-temperature high conductivity reaching 10 $S{\cdot}cm^{-1}$. Furthermore, it is ferromagnetic below 20 K. The ferromagnetic ordering behavior mainly comes from the indirect exchanges between the localized spins of Fe atoms rather than the neighboring Fe atoms.

Being influenced by the above findings, we propose several 2D transition metal-organic frameworks (TM-NH MOF, TM = Sc–Zn) systems using density functional theory (DFT) computations. The geometric construction and stability of these TM-NH MOF structures are firstly investigated. Then, their electronic structures are studied and diagnosed. Lastly, the magnetic properties of TM-NH MOF and their strain effect are systematically discussed. These results could provide a series of 2D MOF materials as potential excellent candidates applied in nanoscale spin electric devices.

2. Methods

The spin-polarized DFT calculations were performed with the Vienna *ab-initio* simulation package (VASP).[38,39] The generalized gradient approximation (GGA) with the Perdew–Burke–Ernzerhof (PBE) was selected to describe the exchange-correlation approximation.[40] The projected augmented wave (PAW) was adopted with the plane-wave cutoff energy of 500 eV.[41] The vacuum layer was larger than 20 Å between the periodically repeated monolayers. The Hellmann–Feynman force on each atom was less than 0.01 $eV{\cdot}Å^{-1}$, and the total energy change was less than 1.0×10^{-5} eV. A dense k-point mesh with a grid density of $2\pi\times0.01$ $Å^{-1}$ in the Monkhorst–Pack scheme was used. To treat the exchange–correlation energy of the localized d-orbital of TM atoms, the PBE+U (U = 3 eV) calculations were employed by adding the Hubbard term to the Hamiltonian.[42,43] The VASPKIT code was used to manipulate the in/output VASP files.[44] The *ab-initio* molecular dynamics (AIMD) was conducted with the Nose algorithm in the *NVT* ensemble.[45]

3. Results and discussion

3.1. Geometry and stability

The unit cell of the studied 2D metal-organic frameworks is built by three transition-metal atoms on graphene with four pyridine-nitrogen-like atoms passivated by H atoms (TM-NH MOF), as shown in Fig. 1, leading to a chemical formula of $TM_3(C_2NH)_{12}$ in a primitive cell. As similar to other 2D MOF materials, TM-NH MOF monolayers are 2D porous carbon-rich materials with one-atom-thickness. The nanosheets of graphene with three high-symmetric sp^2-C atoms (C_1, C_2, C_3) possess large π-bonds, which would enhance the stability of these TM-NH MOF monolayers. The optimized lattice constants of these TM-NH MOF (TM = Sc–Zn) monolayers were calculated by the variation of energies with different lattice constants (Fig. S1). The calculated lattice constants (l_a), bond lengths of TM–N (D_{TM-N}), N–H (D_{N-H}), N–C_1 (D_{N-C1}), C_1–C_2 (D_{C1-C2}), and C_2–C_3 (D_{C2-C3}), and the diameters of the hole (Φ) are summarized in Table 1 and Table S1. The lattice constants of the TM-NH MOF monolayers display a decreased trend for Sc–Co (13.23 Å → 12.52 Å) and an increased trend for Ni–Zn (12.52 Å → 12.95 Å). The bond lengths of N–H (D_{N-H}), N–C_1 (D_{N-C1}), C_1–C_2 (D_{C1-C2}), and C_2–C_3 (D_{C2-C3}) keep the same for different TM-NH MOFs. The bond lengths of TM–N (D_{TM-N}) and the diameters of the hole (Φ) exhibit the same change trend as that of the lattice constants, as transition-metals have different atomic radii. For example, the Sc-NH MOF monolayer possesses the largest lattice constants (13.23 Å) corresponding to the largest atomic radius of Sc atom, consistent with the previous theoretical investigations for other 2D MOF materials.[46,47]

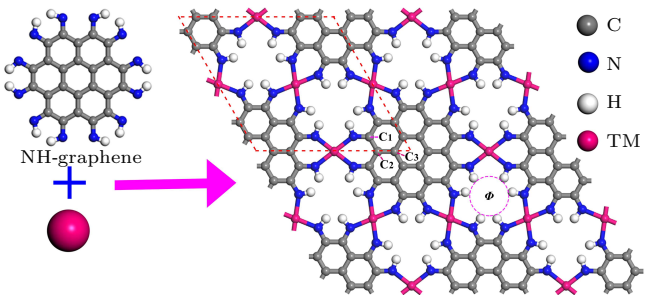


Fig. 1. Schematic atomic structures of 2D TM-NH MOF materials. The red dashed lines outline the unit cell.

Table 1. The geometric parameters [lattice constants (l_a), bond lengths of TM-N (D_{TM-N}), diameters of the hole (Φ)], the binding energy (E_b) per unit cell, and charge transfer of TM (Q_{TM}) and N atoms (Q_N) for different TM-NH MOF monolayers. For Bader charge analysis, + and − denote gaining and losing electrons, respectively.

Materials	l_a (Å)	D_{TM-N} (Å)	Φ (Å)	E_b (eV)	Q_{TM} (e)	Q_N (e)
Sc-NH MOF	13.23	2.08	4.03	−12.31	−1.87	0.95
Ti-NH MOF	12.97	1.98	3.81	−12.84	−1.76	0.92
V-NH MOF	12.88	1.95	3.71	−12.87	−1.39	0.70
Cr-NH MOF	12.79	1.92	3.62	−12.72	−1.33	0.77
Mn-NH MOF	12.71	1.89	3.55	−12.36	−1.46	0.84
Fe-NH MOF	12.61	1.85	3.44	−11.78	−1.27	0.82
Co-NH MOF	12.52	1.82	3.38	−11.23	−0.91	0.72
Ni-NH MOF	12.52	1.82	3.38	−9.95	−0.90	0.78
Cu-NH MOF	12.77	1.92	3.59	−6.93	−0.88	0.75
Zn-NH MOF	12.95	1.99	3.75	−4.78	−1.16	0.92

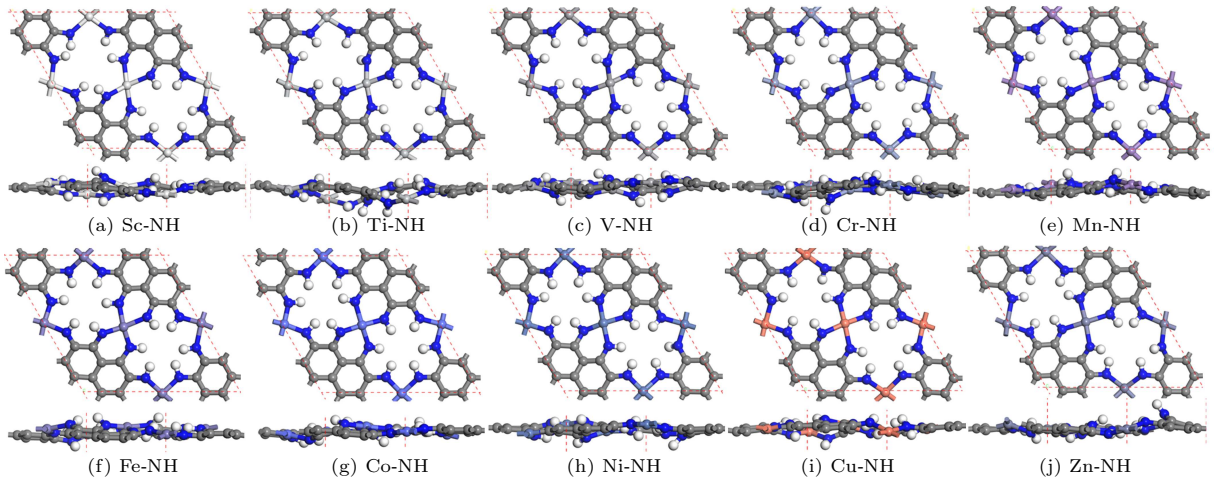


Fig. 2. Top and side views of TM-NH MOF materials after the AIMD simulations at 500 K for 3 ps.

3.2. Electronic property

Both non-magnetic and magnetic configurations were investigated to identify the ground states of TM-NH MOF systems. The spin-polarized energy difference (ΔE_{spin}) between the total energies of non-magnetic and magnetic states was computed by $\Delta E_{spin} = E_{NM} - E_M$, where E_{NM} and E_M are the total energies for non-magnetic and magnetic states, respectively. The calculated spin-polarized energy difference ΔE_{spin} is listed in Table 2. For Ti-, V-, Cr-, Mn-, Fe-, Co-, and Cu-NH MOFs, the ΔE_{spin} values are positive, while for Sc-, Ni-, and Zn-NH MOFs, the ΔE_{spin} values are zero. These results confirm that Ti-, V-, Cr-, Mn-, Fe-, Co-, and Cu-NH MOFs have magnetic ground states and Sc-, Ni-, and Zn-NH MOFs do not have ferromagnetic states.

The electronic band structures of the TM-NH MOF monolayers were explored and plotted in Fig. 3. These 2D TM-NH MOF nanomaterials could exhibit versatile electronic structures. The Ti-, V-, Cr-, Mn-, Fe-, Co-, and Cu-NH MOFs possess spin splitting of band structures, producing magnetism. The Sc-, Ni-, and Zn-NH MOFs do not display spin polarization, according to the spin-polarized energy difference (ΔE_{spin}) and being close to the hexaaminobenzene-derived 2D MOFs.[32] The Sc-, Ti-, V-, Cr-, and Mn-NH MOFs exhibit metallic characters, while Fe-, Co-, Ni-, Cu-, and Zn-NH MOFs are semiconductors (SM), and their band gaps are 0.56 eV, 0.25 eV, 0.41 eV, 0.48 eV, and 0.61 eV, respectively (Table 2). The energy band structures of the Co- and Cu-NH MOFs show a good bipolar magnetic semiconductor (BMS) feature, indicating they could be used for spin generation and injection.[23]

Structural stability is a prerequisite requirement for any practical material. We first calculated the binding energy (E_b) per metal atom of these TM-NH MOF materials by the formula $E_b = (E_{tot} - E_{linker} - E_{TM})/3$, where E_{tot}, E_{linker}, and E_{TM} refer to the total energy of a unit cell, the energies of an isolated organic ligand (NH-graphene) and a TM atom, respectively. From Table 1, it is found that the binding energies (E_b) per metal atom range from −4.78 eV to −12.87 eV, which possess a similar magnitude for $M_3C_{12}S_{12}$,[48,49] $M_3C_{12}N_{12}H_{12}$,[32,50] and $M_3C_{12}O_{12}$.[46,47] These negative binding energies imply that these TM-NH MOF monolayers can be synthesized through appropriate chemical reactions.

To further examine the thermal dynamics of these 2D MOF materials, canonical ensemble-based AIMD simulations were conducted under 500 K for 3000 fs. As shown in Figs. 2 and S2, the variations of the total energy and temperature dur-

ing the whole process display a little oscillation within a fixed value. The AIMD final geometric structures of these TM-NH MOFs show a slight buckling distortion and no bond-breaking, confirming their robust thermal structural stabilities.

The structural stability confirms the effective connection between the TM nodes and NH-graphene organic ligands, which could be further validated by the charge transfer through Bader charge analyses.[51] The Bader charge results are listed in Table 1. The TM atoms lose electrons, while the neighboring N atoms get electrons. The losing electrons of the TM atoms decrease monotonously from Sc to Cu, which is tied to the electronegativity of TM. Generally, the lower electronegativity an element possesses, the more easily it loses electrons. The intense difference in electronegativity of TM and N elements induces strong charge transfer and interaction, which contributes to their robust ionic bonds (Fig. S3).

Table 2. Band structure (BS) (M, HSM, BMS, SM denote metal, half-semiconductor, bipolar magnetic semiconductor, and semiconductor), total magnetic moment M_{T} (μ_{B}) of TM-NH MOF, the magnetic moment of TM atomic basin M_{TM} (μ_{B}) and N M_{N}(μ_{B}) atom for TM-NH MOF systems and the integer values of TM atoms $M_{\mathrm{TM-in}}$ (μ_{B}). ΔE_{spin} (eV) is the energy difference between the total energies for non-magnetic and magnetic states. The spin polarization $P(E_{(\mathrm{F/HOMO})})$ at the Fermi level or the HOMO.

Materials	BS	M_{T}	M_{TM}	$M_{\mathrm{TM-in}}$	M_{N}	ΔE_{spin}	$P(E_{(\mathrm{F/HOMO})})$	E_{gap} (eV)
Sc-NH MOF	M	0	0	1	0	0	0%	0
Ti-NH MOF	M	3.13	0.86	3	−0.016	0.03	6%	0
V-NH MOF	M	7.13	2.05	5	−0.035	1.92	20%	0
Cr-NH MOF	M	9.53	3.31	6	−0.088	3.88	19%	0
Mn-NH MOF	M	9.56	3.48	5	−0.055	3.32	57%	0
Fe-NH MOF	HSM	6.00	2.09	4	−0.019	0.81	100%	0.558
Co-NH MOF	BMS	3.00	1.03	3	−0.018	0.24	100%	0.247
Ni-NH MOF	SM	0	0	2	0	0	0%	0.408
Cu-NH MOF	BMS	3.00	0.61	1	0.079	0.60	100%	0.482
Zn-NH MOF	SM	0	0	0	0	0	0%	0.606

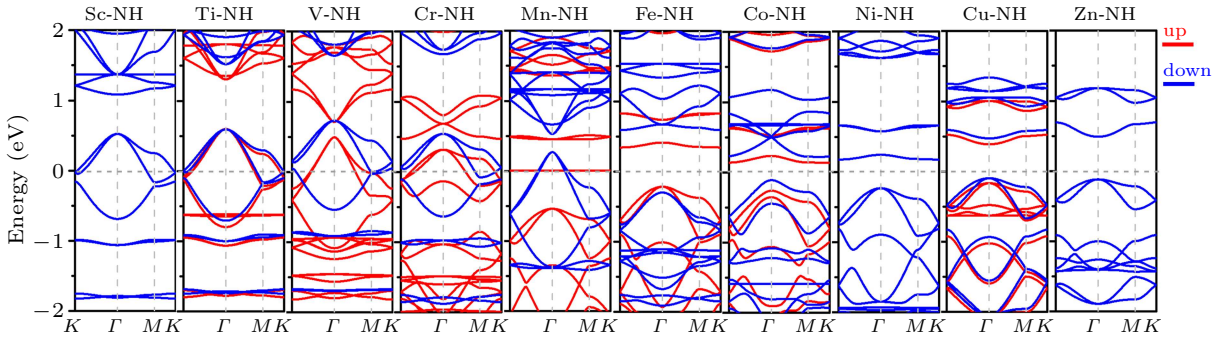


Fig. 3. Band structures of TM-NH MOF monolayers. The Fermi levels (E_{F}) are set to 0 eV.

To better understand the electrical features of TM-MH MOF nano-monolayers, the total density of states (TDOS) is depicted in Fig. 4. The spin-asymmetry of TDOS around the Fermi energy is observable for Ti-, V-, Cr-, Mn-, Fe-, Co-, and Cu-NH MOF monolayers, while the delicate symmetrical TDOS can be found for Sc-, Ni-, and Zn-NH MOF nanosheets, consistent with the band structures.

3.3. Magnetic property

The total magnetic moments (M_{T}) of TM-NH MOF systems, magnetic moments of TM atomic basin (M_{TM}) and N (M_{N}) atom in TM-NH MOF systems are listed in Table 2. For Sc-, Ni-, and Zn-NH MOF systems, the total magnetic moment is zero. Ti-, V-, Cr-, and Mn-NH MOF single layers possess fractional magnetic moments that range from 3.13 μ_{B} to 9.56 μ_{B} due to fractional transfer charges from the TM atoms to the N atoms. While Fe-, Co-, and Cu-NH MOF systems exhibit integer magnetic moments with the values of 6 μ_{B}, 3 μ_{B}, and 3 μ_{B}, respectively, which are similar to the cases for TM-germanene,[52] TM-BeO,[53] and TM-graphdiyne/graphyne.[9] The total magnetic moments (M_{T}) primarily come from the TM atoms (M_{TM}). The total magnetic moments are lower than the corresponding integer values of the TM atoms ($M_{\mathrm{TM-in}}$), which results from the strong interaction between the TM atoms and the NH-graphene.

To investigate spin magnetism of these 2D TM-NH MOF systems, the spin polarization $P(E_{(\mathrm{F/HOMO})})$ at the Fermi level or at the highest occupied molecular orbital (HOMO) was calculated by $P(E_{(\mathrm{F/HOMO})}) = \frac{D(E_{(\mathrm{F/HOMO})\uparrow}) - D(E_{(\mathrm{F/HOMO})\downarrow})}{D(E_{(\mathrm{F/HOMO})\uparrow}) + D(E_{(\mathrm{F/HOMO})\downarrow})}$, where $D(E_{(\mathrm{F/HOMO})\uparrow})$ and $D(E_{(\mathrm{F/HOMO})\downarrow})$ are the spin-up and spin-down density of states at the Fermi level or the HOMO state, respectively. According to the spin polarization $P(E_{(\mathrm{F/HOMO})})$ in Table 2, Fe-, Co-, and Cu-NH MOF monolayers are spin-polarized half-semiconductors (HSM) with 100% spin polarization at the highest valence band (VBM) states, while Ti-, V-, Cr-, and Mn-NH MOF monolayers display metallic (M)

features with 6%, 20%, 19%, and 57% spin polarization. These 2D TM-NH MOF systems have high magnetic moments and spin polarization, suggesting that they could be potential candidates for the application in electronic devices, magnetic recording, and spintronics.

It could be concluded that the different TM atoms in MOF monolayers could effectively tune their magnetic and electronic characteristics. This modulation mainly results from the electron transfer between TM elements and the NH-graphene. From Table 2, obvious charge transfer takes place from TM atoms to NH-graphene ligands, which could not only strengthen the structure stability but also tune the magnetic and electronic properties effectively.

To further study the magnetism of these TM-NH MOF sheets, their spin-charge densities are plotted in Fig. 5. Sc-, Ni-, Zn-NH MOFs have no spin density distribution, suggesting their total magnetic moments M_T being 0 μ_B. In Ti-, V-, Cr-, Mn-, Fe-, and Co-NH MOF materials, the magnetic moments are localized. The spin-up densities are mainly around the TM atoms, while some spin-down densities distribute near the nearest N atoms. In the Cu-NH MOF monolayer, there are some spin-up densities around the N atoms, and spin-up and spin-down densities around the Cu atom, according to the results of magnetic moments depicted in Table 2.

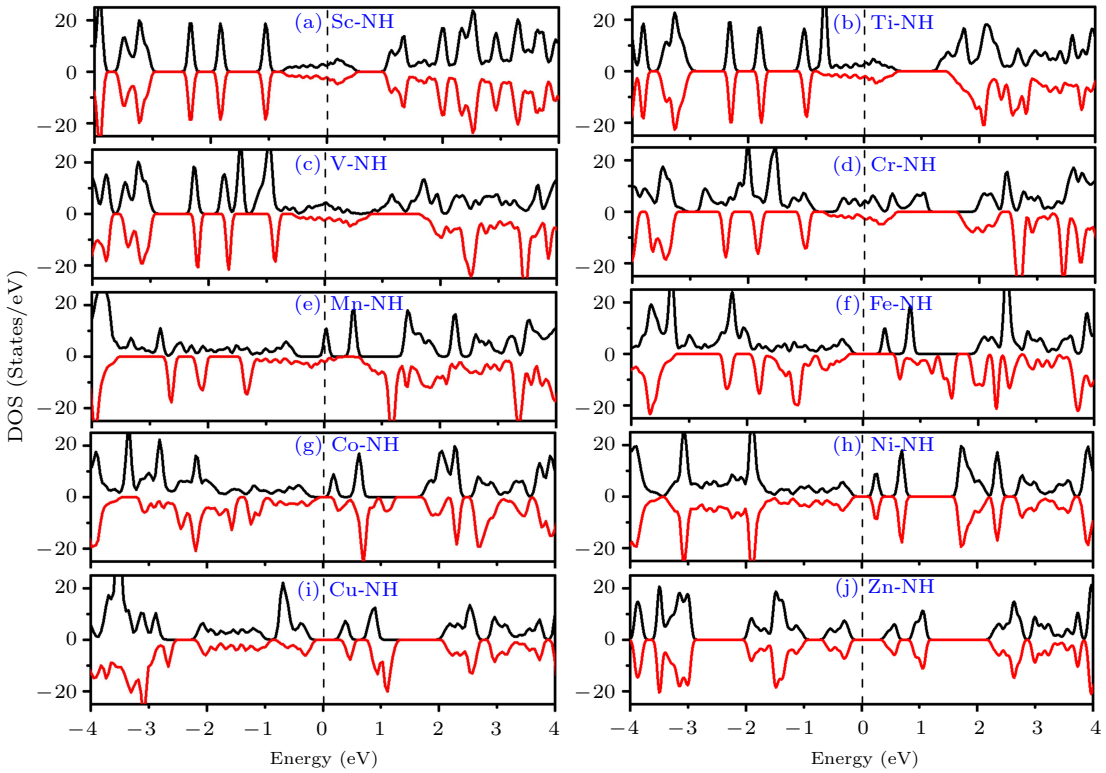


Fig. 4. Total density of states of TM-NH MOF monolayers. The Fermi levels (E_F) are set to 0 eV.

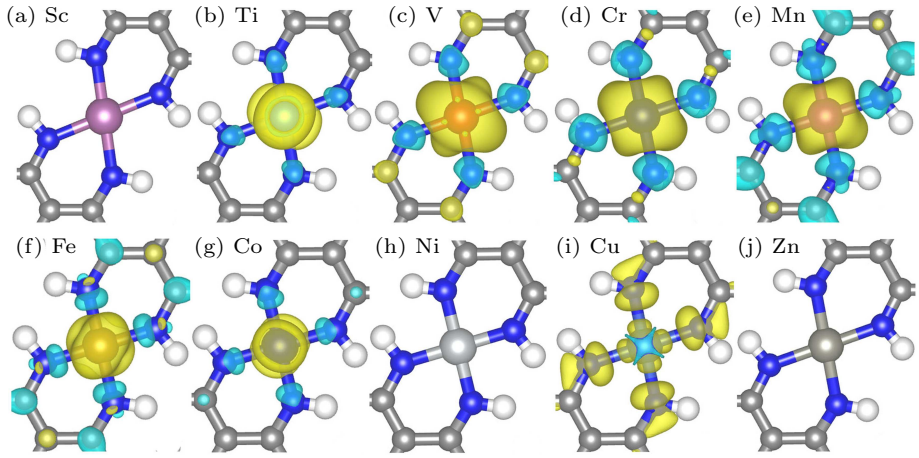


Fig. 5. Spin density distribution for (a)–(j) Sc–Zn TM-NH MOF monolayers. The yellow and blue isosurfaces denote the spin-up and spin-down charge densities, respectively. The isosurface charge density is 0.005 e/Å^3.

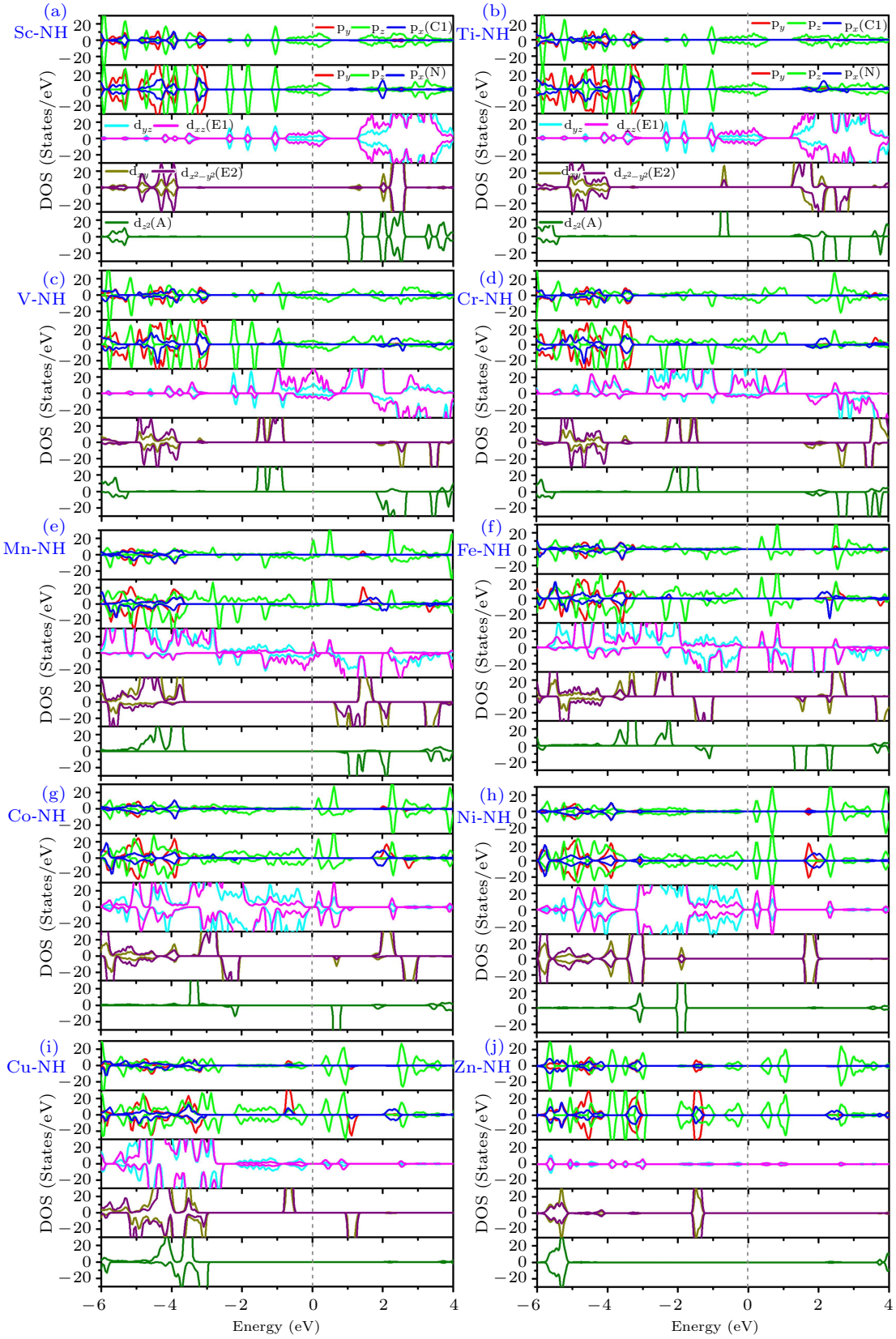


Fig. 6. PDOS of C_1 (denote in Fig. 1), N, and TM in TM-NH MOF monolayers. The Fermi levels (E_F) are set to 0 eV.

We plot the characteristics of projected density of states (PDOS) of the TM, N, and C_1 atoms for all ten TM-NH MOF systems in Fig. 6. For Sc-NH MOF monolayer (Fig. 6(a)), the delicate symmetry of PDOS indicates its nonmagnetic ground state. The N-p_z, C-p_z states significantly overlap with the Sc-E_1 (d_{yz}, d_{xz}) states at Fermi level (E_F), which manifests that the Sc-NH MOF possesses metallic character. As shown in Fig. 6(b), the hybridization between the E_1 (d_{yz}, d_{xz}) orbitals of Ti and p_z orbitals of O/N atoms occurs at the Fermi level (E_F), leading to a metallic character. The giant asymmetry in

the E_2 (d_{xy}, $d_{x^2-y^2}$) and A (d_{z2}) orbitals of Ti atoms results in Ti-NH MOF monolayer becoming original magnetic, agreeing well with the spin density distribution shown in Fig. 5(b). According to the PDOS of V-, Cr-, Mn-NH MOFs in Figs. 6(c)–6(e), they show similar distribution. The E_1 (d_{yz}, d_{xz}) orbitals of TM and p_z orbitals of O/N atoms are split asymmetrically at E_F, which induce the magnetic moments of 7.13 μ_B, 9.53 μ_B, 9.56 μ_B for V-, Cr-, and Mn-NH MOFs, respectively.

The Fe-NH MOF is similar to Co-NH MOF (Figs. 6(f)–6(g)). The p_z and E_1 (d_{yz}, d_{xz}) orbitals are split asymmetrically near the Fermi level, while the p_x, p_y, E_2 (d_{xy}, $d_{x^2-y^2}$) and A (d_{z^2}) orbitals are split asymmetrically far away from the Fermi level, which manifests their spin magnetism. The origins of VBM and CBM of Fe- and Co-NH MOF systems are different. For the Fe-NH MOF monolayer, the VBM and CBM come from the degenerate spin up Fe-d_{yz} and Fe-d_{xz} orbitals. While for the Co-NH MOF single-layer, the VBM and CBM are originated from the degenerate spin-down Co-d_{yz} and spin-up Co-d_{xz} orbitals, respectively. These show that the Fe-NH MOF monolayer is a half-semiconductor (HSM) and Co-NH MOF is a bipolar magnetic semiconductor (BMS). Fe- and Co-NH MOF systems display the same spin polarization of 100% (Table 2), implying that they are potential candidates for spin-electronic devices.

The PDOSs of Ni- and Zn-NH MOF monolayers shown in Figs. 6(h) and 6(j) clearly indicate that the spin-up and spin-down states are symmetric, indicating their nonmagnetic ground states. Their origins of VBM and CBM are different, which are Ni-E_1 (d_{yz}, d_{xz}) and N-p_z for Ni-NH MOF, while C-p_z and N-p_z for Zn-NH MOF. Ni- and Zn-NH MOF monolayers are nonmagnetic semiconductors with band-gap energy of 0.41 eV and 0.61 eV, respectively.

For the monolayer Cu-NH MOF, the spin-up and spin-down PDOSs are asymmetrical, indicating the presence of magnetism. The N-p_z, C-p_z, and E_1 (d_{yz}, d_{xz}) orbitals split asymmetrically and significantly overlap near the Fermi level, leading to the spin-up densities of Cu and N atoms in Cu-NH MOF (Fig. 6(i)). Cu-NH MOF is a bipolar magnetic semiconductor (BMS), the VBM and CBM come from the spin-up N-p_z and spin-down N-p_z orbitals, respectively.

3.4. Strain effect

The 2D MOF materials possess a large dynamical range of exerting elastic strain, which could encourage them in the application of flexible spintronic devices.[54–56] The biaxial strain is defined by $\varepsilon = \Delta c/c_0$, where the lattice constants of the pristine and strained supercells are c_0 and $c = c_0 \pm \Delta c$, respectively. Here, the $+|\varepsilon|$ and $-|\varepsilon|$ represent tensile strain and compressive strain, respectively. The strain range from -5% to $+5\%$ was considered according to their mechanical strength and the previous reports, and the corresponding variations of the total magnetic moment (M_T) of TM-NH MOF structures were calculated and shown in Fig. 7. The strain can not induce the magnetism of Sc-, Ni-, and Zn-NH MOF systems, they still stay in the nonmagnetic ground state (Table S2). The strain also does not affect the total magnetic moments of Fe- and Co-NH MOFs, they remain at 6 μ_B and 3 μ_B, respectively. Interestingly, Cr-NH MOF has an approximately linear correlation between the total magnetic moment and strain (-5% to $+5\%$). For V- and Ti-NH MOF monolayers, there is a slight increase from compressive strain of -5% to tensile strain of $+5\%$. The Cu-NH MOF sheet exhibits a total magnetic moment of 1 μ_B under the strain of -5% to -3%, and a total magnetic moment of 3 μ_B under the strain of -1% to $+5\%$. Furthermore, the PDOS of E_1 (d_{yz}, d_{xz}), E_2 (d_{xy}, $d_{x^2-y^2}$) and A (d_{z^2}) of the TM atoms in TM-NH MOFs under the different strain were calculated and shown in Fig. S4. The PDOS display different overlap near E_F under different strain, leading to the variation in the total magnetic moments. The results confirm that strain engineering is an effective strategy to tune the electric and magnetic characters of nanomaterials.

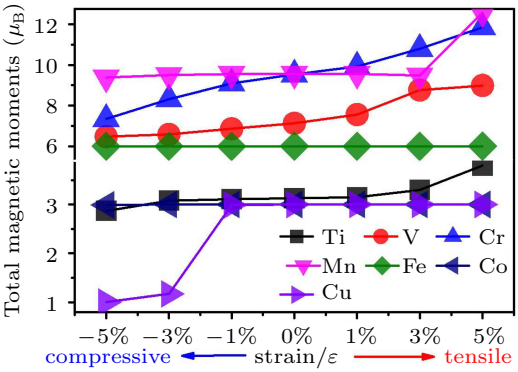


Fig. 7. Magnetic moments of TM-NH MOF monolayers under the strain from -5% to 5%.

4. Conclusion

In summary, a series of 2D MOF materials $TM_3(C_2NH)_{12}$ are investigated by DFT calculations. The binding energies and AIMD indicate that these ten TM-NH MOF (TM = Sc–Zn) monolayers possess excellent structural stability, which results from the charge transfer and strong interaction between TM and NH-graphene. The optimized lattice constants of the TM-NH MOF monolayer are 12.52 Å–13.23 Å, which is dependent on the atomic radii of the transition-metal atoms. These TM-NH MOF monolayers exhibit different magnetic and electronic characters. Sc-, Ti-, V-, Cr, and Mn-NH MOFs are metallic, while Ni- and Zn-NH MOFs exhibit semiconductors (SM) with band gaps of 0.41 eV and 0.61 eV, respectively. Co- and Cu-NH MOF nanomaterials are good bipolar magnetic semiconductors (BMS). Fe-NH MOF monolayer is a half-semiconductor (HSM). The central transition metal atom could effectively modulate the magnetic property of TM-NH MOFs, especially the different spin polarized d-orbitals of

the TM atoms. The effect of elastic strain on the magnetic and electronic characters is studied under strain (from −5% to +5%). The results testify that charge redistribution of TM-3d states is responsible for the magnetic transformation under different elastic strains. This work proposes a new class of 2D MOF materials, and could shed light on the development of 2D magnetic materials.

Acknowledgment

The authors thank the high performance computing center of Henan Normal University, and national super computing center in Zhengzhou.

References

[1] Mei L, Zhu S, Yin W, Chen C, Nie G, Gu Z and Zhao Y 2020 *Theranostics* **10** 757
[2] Tan C, Cao X, Wu X, He Q, Yang J, Zhang X, Chen J, Zhao W, Han S, Nam G, Sindoro M and Zhang H 2017 *Chem. Rev.* **117** 6225
[3] Wang Y, Wang L, Zhang X, Liang X, Feng Y and Feng W 2021 *Nano Today* **37** 101059
[4] Yang C, Wang H and Xu Q 2020 *Chem. Res. Chin. U.* **36** 10
[5] Li D, Gong Y, Chen Y, Lin J, Khan Q, Zhang Y, Li Y, Zhang H and Xie H 2020 *Nano. Micro. Lett.* **12** 36
[6] Jin H, Guo C, Liu X, Liu J, Vasileff A, Jiao Y, Zheng Y and Qiao S 2018 *Chem. Rev.* **118** 6337
[7] Stankovich S, Dikin D A, Dommett G H B, Kohlhaas K M, Zimney E J, Stach E A, Piner R D, Nguyen S T and Ruoff R S 2006 *Nature* **442** 282
[8] Zhou M, Lu Y, Cai Y, Zhang C and Feng Y 2011 *Nanotechnology* **22** 385502
[9] He J, Ma S Y, Zhou P, Zhang C X, He C and Sun L Z 2012 *J. Phys. Chem. C* **116** 26313
[10] Du J, Xia C, An Y, Wang T and Jia Y 2016 *J. Mater. Sci.* **51** 9504
[11] Roy D, Hossain M K, Hasan S M, Milon, Hossain M A and Ahmed F 2021 *Physica E* **125** 114359
[12] Li S, Zhou M, Li M, Lu G, Wang X, Zheng F and Zhang P 2018 *J. Appl. Phys.* **123** 95110
[13] Yu W, Zhu Z, Niu C, Li C, Cho J and Jia Y 2016 *Nnanscale Res. Lett.* **11** 77
[14] Huang B, Clark G, Navarro-Moratalla E, Klein D R, Cheng R, Seyler K L, Zhong D, Schmidgall E, McGuire M A, Cobden D H, Yao W, Xiao D, Jarillo-Herrero P and Xu X 2017 *Nature* **546** 270
[15] Gong C, Li L, Li Z, Ji H, Stern A, Xia Y, Cao T, Bao W, Wang C, Wang Y, Qiu Z Q, Cava R J, Louie S G, Xia J and Zhang X 2017 *Nature* **546** 265
[16] An Y, Wang K, Gong S, Hou Y, Ma C, Zhu M, Zhao C, Wang T, Ma S, Wang H, Wu R and Liu W 2021 *npj Comput. Mater.* **7** 45
[17] Deng Y, Yu Y, Song Y, Zhang J, Wang N, Sun Z, Yi Y, Wu Y, Wu S, Zhu J, Wang J, Chen X and Zhang Y 2018 *Nature* **563** 94
[18] Lin H, Yan F, Hu C, Lv Q, Zhu W, Wang Z, Wei Z, Chang K and Wang K 2020 *ACS Appl. Mater. Interfaces* **12** 43921
[19] Hu C, Zhang D, Yan F, Li Y, Lv Q, Zhu W, Wei Z, Chang K and Wang K 2020 *Sci. Bull.* **65** 1072
[20] Tang X and Kou L 2019 *J. Phys. Chem. Lett.* **10** 6634
[21] Zhu G and Sun Q 2016 *Comp. Mater. Sci.* **112** 492
[22] Deng Y, Yu Y, Song Y, Zhang J, Wang N Z, Sun Z, Yi Y, Wu Y, Wu S, Zhu J, Wang J, Chen X and Zhang Y 2018 *Nature* **563** 94
[23] Li X and Yang J 2016 *Natil. Sci. Rev.* **3** 365
[24] Song X, Liu J, Zhang T and Chen L 2020 *Sci. China Chem.* **63** 1391
[25] Li C, Zhang L, Chen J, Li X, Sun J, Zhu J, Wang X and Fu Y 2021 *Nanoscale* **13** 485
[26] Yu M, Dong R and Feng X 2020 *J. Am. Chem. Soc.* **142** 12903
[27] Zhao W, Chen T, Wang W, Jin B, Peng J, Bi S, Jiang M, Liu S, Zhao Q and Huang W 2020 *Sci. Bull.* **65** 1803
[28] Cai D, Lu M, Li L, Cao J, Chen D, Tu H, Li J and Han W 2019 *Small* **15** 1902605
[29] Song X, Wang X, Li Y, Zheng C, Zhang B, Di C A, Li F, Jin C, Mi W, Chen L and Hu W 2020 *Angew. Chem. Int. Edit.* **59** 1118
[30] Jiang Q, Xiong P, Liu J, Xie Z, Wang Q, Yang X Q, Hu E, Cao Y, Sun J, Xu Y and Chen L 2020 *Angew. Chem. Int. Edit.* **59** 5273
[31] Wu Z, Adekoya D, Huang X, Kiefel MJ, Xie J, Xu W, Zhang Q, Zhu D and Zhang S 2020 *ACS Nano* **14** 12016
[32] Mortazavi B, Shahrokhi M, Makaremi M, Cuniberti G and Rabczuk T 2018 *Mater. Today Energy* **10** 336
[33] Chakravarty C, Mandal B and Sarkar P 2016 *J. Phys. Chem. C* **120** 28307
[34] Chakravarty C, Mandal B and Sarkar P 2019 *J. Phys. Chem. C* **124** 37
[35] Zhao M, Wang A and Zhang X 2013 *Nanoscale* **5** 144
[36] Liu J and Sun Q 2015 *ChemPhysChem* **16** 614
[37] Dong R, Zhang Z, Tranca D C, Zhou S, Wang M, Adler P, Liao Z, Liu F, Sun Y, Shi W, Zhang Z, Zschech E, Mannsfeld S C B, Felser C and Feng X 2018 *Nat. Commun.* **9** 2637
[38] Kresse G and Hafner J 1993 *Phys. Rev. B* **47** 558
[39] Kresse G and Furthmüller J 1996 *Phys. Rev. B* **54** 11169
[40] Perdew J P, Burke K and Ernzerhof M 1998 *Phys. Rev. Lett.* **77** 3865
[41] Kresse G and Joubert D 1999 *Phys. Rev. B* **59** 1758
[42] Chanier T, Sargolzaei M, Opahle I, Hayn R and Koepernik K 2006 *Phys. Rev. B* **73** 134418
[43] Wehling T O, Lichtenstein A I and Katsnelson M I 2011 *Phys. Rev. B* **84** 235110
[44] Wang V, Xu N, Liu J C, Tang G and Geng W 2021 *Comput. Phys. Commun.* 108033
[45] Martyna G J, Klein M L and Mark T 1992 *J. Chem. Phys.* **97** 2635
[46] Wang P, Jiang X, Hu J, Wang B, Zhou T, Yuan H and Zhao J 2020 *Phys. Chem. Chem. Phys.* **22** 11045
[47] Zhang J, Zhou Z, Wang F, Li Y and Jing Y 2020 *ACS Sustain. Chem. Eng.* **8** 7472
[48] Baidya S, Kang S, Kim C H and Yu J 2019 *Sci. Rep.* **9** 13807
[49] Tian Y, Zhu C, Yan L, Zhao J and Su Z 2019 *J. Mater. Chem. A* **7** 15341
[50] Cui Q, Qin G, Wang W, Geethalakshmi K R, Du A and Sun Q 2020 *Appl. Surf. Sci.* **500** 143993
[51] Henkelman G, Arnaldsson A and Jónsson H 2006 *Comp. Mater. Sci.* **36** 354
[52] Sun M, Ren Q, Wang S, Zhang Y, Du Y, Yu J and Tang W 2016 *Comp. Mater. Sci.* **118** 112
[53] Song N H, Wang Y S, Zhang LY, Yang Y Y and Jia Y 2018 *J. Magn. Magn. Mater.* **468** 252
[54] Xu Z, Hou Q, Guo F, Jia X, Li C and Li W 2018 *Curr. Appl. Phys.* **18** 1465
[55] Wu N, Zhao X and Wang T 2016 *Physica E* **84** 505
[56] Liu J, Ma Y, Zhao M, Yi L, Dai X and Tang Y 2018 *J. Mater. Sci.* **53** 5114